



Aalborg Universitet

AALBORG UNIVERSITY
DENMARK

The role of turbulence in the deposition of intrinsically buoyant MPs

Molazadeh, Marziye; Calabro, Guilherme; Liu, Fan; Tassin, Bruno; Rovelli, Lorenzo; Lorke, Andreas; Dris, Rachid; Vollertsen, Jes

Published in:
Science of the Total Environment

DOI (link to publication from Publisher):
[10.1016/j.scitotenv.2023.168540](https://doi.org/10.1016/j.scitotenv.2023.168540)

Creative Commons License
CC BY 4.0

Publication date:
2024

Document Version
Publisher's PDF, also known as Version of record

[Link to publication from Aalborg University](#)

Citation for published version (APA):
Molazadeh, M., Calabro, G., Liu, F., Tassin, B., Rovelli, L., Lorke, A., Dris, R., & Vollertsen, J. (2024). The role of turbulence in the deposition of intrinsically buoyant MPs. *Science of the Total Environment*, 911, Article 168540. <https://doi.org/10.1016/j.scitotenv.2023.168540>

General rights

Copyright and moral rights for the publications made accessible in the public portal are retained by the authors and/or other copyright owners and it is a condition of accessing publications that users recognise and abide by the legal requirements associated with these rights.

- Users may download and print one copy of any publication from the public portal for the purpose of private study or research.
- You may not further distribute the material or use it for any profit-making activity or commercial gain
- You may freely distribute the URL identifying the publication in the public portal -

Take down policy

If you believe that this document breaches copyright please contact us at vbn@aub.aau.dk providing details, and we will remove access to the work immediately and investigate your claim.



The role of turbulence in the deposition of intrinsically buoyant MPs

Marziye Molazadeh (Shabnam)^{a,*}, Guilherme Calabro^b, Fan Liu^a, Bruno Tassin^b,
Lorenzo Rovelli^c, Andreas Lorke^c, Rachid Dris^b, Jes Vollertsen^a

^a Aalborg University, Section of Civil and Environmental Engineering, Department of the Built Environment, Thomas Manns Vej 23, 9220 Aalborg Øst, Denmark

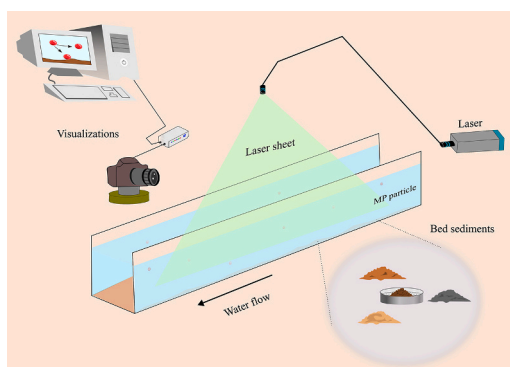
^b LEESU, Ecole des Ponts, Univ Paris Est Creteil, Marne-la-Vallée, France

^c Institute for Environmental Sciences, RPTU Kaiserslautern-Landau, Landau, Germany

HIGHLIGHTS

- Experimental validation on mixing induced transfer of MPs from water surface to sediments.
- Substantial quantity of PE particles was subject to downward vertical transport.
- Vertical velocity of PE in turbulent flows varied over 4 orders of magnitude from predicted rising velocity in still water.

GRAPHICAL ABSTRACT



ARTICLE INFO

Editor: Damia Barcelo

Keywords:
Buoyant MPs
Vertical transport
Turbulent flow
PTV

ABSTRACT

Intrinsically floating microplastics (MP) such as polyethene (PE) or polypropylene (PP) are among the most common MPs found in aquatic sediments. There must hence be mechanisms that cause lighter-than-water MPs to deposit despite them being buoyant. How these MPs end up in the sediment bed is only partly understood. This study explores how turbulence in the water can affect the vertical movement of buoyant MP and bring them in contact with the bed. The deposition of PE (995 kg m^{-3}) in slow-flowing water (average flow velocities of 1.85 and 4.17 cm s^{-1}) was measured by tracking them and analyzing their motion in an open, rectangular, glass-sided flume. Flow characteristics in terms of turbulent kinetic energy and shear velocity were measured by particle image velocimetry. Experiments were conducted at a water depth of 27 cm and at various hydraulic conditions created by adjusting inflow speeds and using different bed materials: medium gravel, fine gravel, medium sand, cohesive sediment, and glass. The results showed that the vertical velocity of the MPs in the turbulent flow regimes varied over 4 orders of magnitude from their predicted rising velocity in quiescent water (laminar flow). Turbulence mixing resulted in distribution throughout the water column with a substantial quantity consistently subject to downward vertical transport, which in turn increased the chance of the PE particles encountering the bed and potentially getting immobilized. This work provides a plausible explanation and further experimental

* Corresponding author.

E-mail address: marziyem@build.aau.dk (M. Molazadeh).

<https://doi.org/10.1016/j.scitotenv.2023.168540>

Received 29 July 2023; Received in revised form 22 October 2023; Accepted 10 November 2023

Available online 19 November 2023

0048-9697/© 2023 The Authors. Published by Elsevier B.V. This is an open access article under the CC BY license (<http://creativecommons.org/licenses/by/4.0/>).

validation for the concept of mixing induced transfer of MPs from the water surface to the sediments of shallow waters.

1. Introduction

Plastic pollution in the aquatic environment causes major problems, ranging from macroscopic impacts such as the entanglement of marine wildlife by macroplastics (>5 mm), to the ingestion of tiny plastic fragments called microplastics (MPs) (<5 mm) by organisms. Plastic pollution is linked to its widespread use and inadequate practices in waste management, as well as the physical properties of plastics such as durability and floating ability. These properties result in their easy transport in water bodies (Moore, 2008).

With growing concern about the adverse environmental impacts of plastics, this topic has seen increasing interest from the public, from legislators, and researchers. There has been a particular focus on MPs due to their potential harm to organisms. These particles are released into the environment either as primary MPs (i.e., as plastic particles intentionally produced to sizes below 5 mm) (Cole et al., 2011) or from the fragmentation of larger plastic items under impact of light, heat, mechanical forces, and other factors (secondary MPs) (Andrady, 2011).

Studies of MPs in various water bodies have shown that they cover a wide spectrum of properties in terms of polymer, size, shape, density, etc. which all affect their mobility and eventual fate (Khatmullina and Chubarenko, 2019). MPs in a flowing water body, for example a river (Lu et al., 2023) or the currents of a lake (Yan et al., 2022) or ocean (Liu et al., 2023), can be transported longitudinal over long distances. At the same time, they are transported vertically due to gravitational forces and the eddies of turbulent flow (Molazadeh et al., 2023). The vertical transport ultimately leads to the MPs arriving at the bottom of the water body, where they can become part of the sediment bed (Simon-Sanchez et al., 2022).

One of the physical characteristics commonly associated with the mobility and fate of MPs is their density. The density of MPs varies widely, with some having densities as low as 0.8 g cm^{-3} and others as high as 2 g cm^{-3} (Koelmans et al., 2022). Positively buoyant MPs are lighter than the ambient fluid; hence based on the density alone, they are supposed to be present at the surface of a water body and not close to or in its bed. Nevertheless, lower-than-water-density polymers such as PP and PE are among the most common MPs found in freshwater sediments (Molazadeh et al., 2023; Olesen et al., 2019; Liu et al., 2019).

MP density, and consequently their sinking behavior, have been widely reported to change in the environment due to various mechanisms, such as material ageing, biofouling, aggregation with other organic/inorganic particles, vertical mixing, etc. (Long et al., 2015; Semcesen and Wells, 2021; Molazadeh et al., 2023). However, a recent paper by Jalón-Rojas et al. (2022) contradicts the general assumption that the attachment of biofilm to a plastic particle will result in faster descent. The authors showed that the irregular attachment of biofilm decreased the sinking velocity of sheets due to triggering motion instabilities, despite an increase in density. These and other findings (Besseling et al., 2017; Li et al., 2019) indicate that processes other than simple sinking or rising can affect the vertical transport of MPs, and that they should be given more attention.

Another process which can affect the vertical transport of MPs is turbulence-induced mixing driven by factors such as surface wind, temperature gradients, river flow, and waves, as they cause motion in addition to gravity and buoyancy, which then affects the fate of particles (Shamskhany and Karimpour, 2022). However, so far, physical drivers of MP transport within turbulent aquatic environments have only sporadically been investigated. The gravitational velocity of MPs in quiescent water has been examined by several researchers (Ballent et al., 2013; Reisser et al., 2015; Kowalski et al., 2016; Khatmullina and Isachenko, 2017; Kaiser et al., 2019; Waldschläger and Schüttrumpf,

2019). However, water bodies like rivers and the upper layers of lakes, fjords, and seas are not quiescent (laminar flow conditions) but turbulent, and experimental studies of the vertical velocity of MPs under such conditions are scarce. Studies addressing turbulent conditions have been limited to modelling exercises (Daily and Hoffman, 2020; Shamskhany and Karimpour, 2022). For example, in the study by Shamskhany and Karimpour (2022), the authors modelled the effect of MP size and density on their mixing behavior in response to different turbulence intensities, and they found that the motion of small MPs is highly influenced by the ambient turbulent flow. Additionally, field measurements (Kukulka et al., 2012; Kooi et al., 2016) as well as regional large-eddy simulations of oceans (Liang et al., 2012; Yang et al., 2014; Brunner et al., 2015; Taylor, 2018) have shown the presence of vertical concentration profiles within the ocean mixed layer. These profiles are largely caused by wind and wave breaking at the ocean surface (Chamecki et al., 2019), leading to buoyant particles being distributed in the ocean mixed layer instead of accumulating at its surface.

Moreover, whether turbulence can transfer buoyant MPs from the water surface to the sediments has not yet been experimentally investigated. In a study by Molazadeh et al. (2023) the authors concluded that mixing was likely to have caused the transfer of PP and PE polymers to the bed sediments of a small water body. They substantiated this by computational fluid dynamics modelling. However, to prove this concept, in-depth laboratory experiments are needed. Studying this fundamental mechanism can help to answer the question of why much plastic seems to be missing in the global plastic mass budget. The lack of balance between plastic production and observed plastic in the oceans (Isobe and Iwasaki, 2022) suggests the possibility of buoyant polymers existing in the water column and entering the sediments rather than staying at the water surface. Furthermore, understanding the role of turbulence in MP transport is a prerequisite to predict the pathways and final endpoints of MPs in water bodies, which in turn will allow better estimates on local concentrations and consequently environmental impacts.

The objective of this study was to better understand the turbulent transport of buoyant MPs. It was done by tracking the movement of marginally buoyant MPs (PE particles) under turbulent flow conditions to see how the ambient flow regime and conditions affect their movement. The probability that a particle can encounter the bed at different flow turbulent kinetic energies and bed types was also assessed. For this, Particle Tracking Velocimetry (PTV) and Particle Image Velocimetry (PIV) were applied to separately monitor the trajectory and velocities of individual PE particles and measure turbulence characteristics. Different sets of experiments with different flow conditions and bed types were conducted.

2. Material and methods

2.1. Experimental setup and experimental conditions

The experiments were conducted in a 2 m long, 0.3 m wide, and 0.3 m deep, rectangular, glass-sided, flume in the hydraulics laboratory of the National Research Institute for Agriculture, Food and the Environment (INRAE) at Antony, France (Fig. 1). For all experiments, the flume was filled to a height of $h = 27 \text{ cm}$ with tap water with a measured density of 1001 kg m^{-3} . Five test beds were examined, ranging from a glass bed (no sediment in the flume) to a gravel bed (Table 1). The size distribution of each bed sediment can be seen in Fig. S1. Before each experiment, sediments were washed until the residual water was clear. It was necessary to remove dirt from the medium gravel, fine gravel, and medium sand beds as it otherwise could have interfered with the flow

analysis. The cohesive sediments consisted of clay and silt. The sediment size distribution for this bed type was found by laser diffraction. The median grain diameters (d_{50}) of the beds are given in Table 1. Each bed was established at the bottom of the flume with a thickness of 0.05 m. The test section was located 1.2 m downstream of the water inlet (Fig. 1). The water temperature was around 20 °C throughout the experiments.

Water entered the flume through 2 customized pipes, placed 1.2 m upstream of the measuring location (Fig. 1A). The pipes were parallel, horizontal, and had holes pointing in the direction of the flow (Fig. 1B). At its lowest and highest level, the pump generated a flow resulting in an average velocity in the flume of 1.85 and 4.17 cm s⁻¹, corresponding to Reynolds numbers of 3674 and 8282, respectively. The flow conditions created when the pump was set at its highest and lowest level are subscripted with respectively 1 and 2 in Table 1. In addition, to create a less turbulent flow condition at the lowest flow rate, the inflow pipes (Fig. 1B) were turned in the opposite direction of the flow, that is, the holes pointed towards the upstream flume wall. By hitting the wall and being reflected back into the flume, some of the energy of the flow was dissipated, creating less turbulence. This flow condition is subscripted with 3 in Table 1.

2.2. Measuring particle trajectories

Instantaneous velocities for each test were measured by two-dimensional particle image velocimetry (PIV). The flow was seeded with small tracer particles and illuminated with a pulsed laser light sheet. A camera recorded images of the illuminated area during each light pulse. The displacement of the particle between the light pulses was used to determine the velocity vectors. A high-speed camera (Dantec Dynamics FlowSense 4 M (CCD) digital camera) with a resolution of 2048 × 2048 pixels and an Nd: YAG double-pulse laser (Litron Lasers Nano —S200 15 PIV, wavelength: 532nm), fitted with a Powell lens line optics to generate a planar light sheet, was used for the PIV measurements.

The measurements were conducted in the vertical centerline of the flume at a distance of 15 cm from the side walls, and the field of view (FOV) was irradiated by the laser. The thickness of the laser sheet was approximately 1 mm, and it entered the flow through the free surface allowing simultaneous measurements of the streamwise (u) and wall-normal velocity components (v).

The seeding particles to trace the flow, and thus measure flow characteristics according to their instantaneous motion, were 20 μm Polyamide particles (PSP) with a specific gravity of 1030 kg m⁻³. A calibration target was used to provide a reference scale for the physical dimensions in the captured images and the corresponding distances in the real-world flow field. The camera recorded double-frame images for 90 s at a rate of 7.4Hz within the FOV of approximately 6 × 6 cm. The FOV varied between 5.6 and 6.4 cm for different experiments, and was

calculated from calibration images that captured the water from ~1 cm above the bed. The time interval between each frame, i.e., between laser pulses, was 22 ms. The image pairs were processed using the open-source software PIVlab (Thielicke and Stamhuis, 2014). An FFT deformation algorithm (direct Fourier transform correlation with multiple passes and deforming windows) was used within the PIVlab software to derive the velocity field. The data were analyzed by this algorithm in 3 passes with 128, 64, and 32-pixel interrogation areas (Thielicke and Stamhuis, 2014).

To track the path of MPs and measure their velocity, 40–47 μm spherical and fluorescent PE particles (UVPMS-BR, Cospheric) with a density of 995 kg m⁻³ were injected into the flume, and their trajectories tracked. The laser sheet for illuminating the fluorescent particles was approximately 2 cm deep. The particles emitted light in a red color when excited by the laser, clearly distinguishing them from other particles in the flow. A long-pass optical filter was mounted on the camera lens to capture only the emitted (fluorescent) red light from the MP particles.

At the start of each experiment, the FOV was checked to see how many particles were left from previous experiments. Depending on the leftover particle concentration, approx. 8.5 mg of fluorescent particles was dispersed in a small amount of water and added to the flume. This step involved some trial-and-error checking of the FOV to see if there were enough particles to be tracked, as some particles got stuck in the tubing's and other parts of the flume, thus leading to some loss of particles.

A series of images was recorded at 14.8 Hz for 30 s. Because the images were taken rapidly, individual MPs could be tracked and followed over the time of measurement while passing the FOV. Each measurement was repeated 6 times, for a total of 3 min per experiment. The sequences of captured images were processed to identify and track individual particles over time using algorithms developed by Stanford University to track the trajectories of particles moving in fluids (Particle Tracking, Stanford). The image processing toolbox of MATLAB (MathWorks) was used to pre-process images, for instance, to increase image intensities or to draw the bed topography.

2.3. Particle transport

Turbulence data were computed based on the fluctuating velocity obtained from a classical Reynolds decomposition; that is, the instantaneous horizontal and vertical velocity components were decomposed into a mean value and a fluctuation term (Eq. (1); Reynolds, 1895). Data from the PIV measurements provided the streamwise, u , and wall-normal, v , instantaneous flow velocity fields.

$$u' = u - \bar{u} \text{ and } v' = v - \bar{v} \quad (1)$$

where u and v are the instantaneous velocity components, \bar{u} and \bar{v} the time-averaged components, and the primes indicate their fluctuation

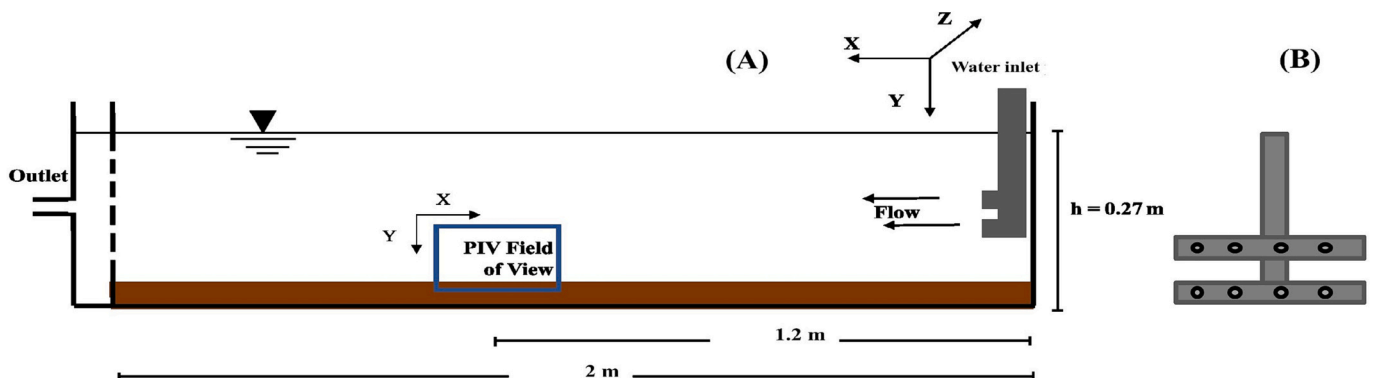


Fig. 1. Schematic of the experimental set-up (A) front view of the customized water inlet pipe (B).

terms. The turbulent kinetic energy (TKE, Eq. (2)) was used to quantify the intensity of the turbulent flow. The lateral velocity component is not measured by 2D PIV, and 2D PIV hence provides velocity information in a plane only, meaning in the streamwise-vertical plane, neglecting the lateral velocity component. The estimated TKE could hence not fully account for the energy associated with the lateral turbulence.

$$TKE = \frac{1}{2} (\overline{u'^2} + \overline{v'^2}) \tag{2}$$

To investigate entrainment of hypothetical particle sizes and densities not physically tested in the flume experiments, the dimensionless Rouse parameter was introduced (Eq. (3)).

$$P = \frac{W_s}{\beta K u^*} \tag{3}$$

where W_s is the particle terminal settling/rising velocity [$m s^{-1}$], k is the von Karman constant [-] set to 0.4, β [-] is a parameter that adjusts the assumption of parabolic eddy diffusivity for the Rouse profile (assumed to be 1) (De Leeuw et al., 2020), and u^* is the spatially averaged shear velocity [$m s^{-1}$] of the flow calculated from Eq. (4).



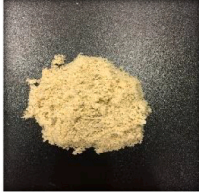

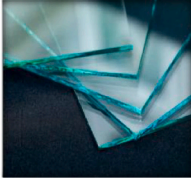
$$u^* = \sqrt{\overline{u'v'}} \tag{4}$$

To calculate the Rouse parameter, the particle terminal velocity (W_s) must be derived. For small spherical particles, like the 40–47 μm PE particles of the present study, W_s can be determined by Stokes law (Eq. (5)) as it is valid for spherical particles $<100 \mu m$.

$$W_s = \frac{gd^2(\rho_p - \rho_w)}{18\mu} \tag{5}$$

Table 1

Investigated flow conditions and bed types, TKE (turbulent kinetic energy), u^* (shear velocity) and d_{50} (median grain diameter of the sediment bed) of each experiment.

Test bed / Flow condition	TKE (J/kg)	u^* (cm/s)	d_{50} (mm)	Bed types
Medium gravel 1	6.9×10^{-4}	0.7	8.3284	
Medium gravel 2	3.8×10^{-4}	0.5	8.3284	
Medium gravel 3	2.6×10^{-4}	0.48	8.3284	
Fine gravel 1	6.6×10^{-4}	1.05	3.2288	
Fine gravel 2	8.0×10^{-4}	0.95	3.2288	
Fine gravel 3	2.6×10^{-4}	0.47	3.2288	
Medium sand 1	5.0×10^{-4}	0.8	0.2641	
Medium sand 2	3.0×10^{-4}	0.65	0.2641	
Medium sand 3	6.3×10^{-4}	0.49	0.2641	
Cohesive sediment 1	N.A.	N.A.	0.0336	
Cohesive sediment 2	N.A.	N.A.	0.0336	
Cohesive sediment 3	N.A.	N.A.	0.0336	
Glass 1	1.2×10^{-3}	1.26	-	
Glass 2	6.1×10^{-4}	0.62	-	
Glass 3	8.7×10^{-4}	0.86	-	

where g is the gravitational acceleration [$m\ s^{-2}$], d the particle diameter [m], f_p the particle density [$kg\ m^{-3}$], f_w the density of the ambient water [$kg\ m^{-3}$], and μ is the kinematic viscosity [$m^2\ s^{-1}$] of the flow at $20\ ^\circ C$.

For larger particles, the Dietrich formula (Dietrich, 1982) was used to calculate the particle settling or rise velocity, as it is valid for particles up to 4.9 mm. Only spherical particles were considered, and the Dietrich formula could be simplified to Eq. (6) (Isachenko, 2020).

$$W_s = \sqrt[3]{W_s \frac{(f_p - f_w)}{(\rho_w)^2} - g\mu} \tag{6}$$

where

$$W_s = 10^R$$

$$R = -3.76715 + 1.92944\log_{10}D_s - 0.09815(\log_{10}D_s)^2 - 0.00575(\log_{10}D_s)^3 + 0.00056(\log_{10}D_s)^4$$

$$D_s = \frac{|f_p - f_w| g d^3 f_w}{\mu^2}$$

3. Results and discussion

3.1. Measured flow characteristics

The measured flow characteristics, including turbulent kinetic energy (TKE) and shear velocity (u^*), did not increase with bed roughness (Table 1). There were several reasons for this. One was that the flume was too short (2 m) to ensure a fully developed velocity profile, that is, the upstream and downstream discharge points affected the flow pattern and hence the measurements. The bed form with its undulations could in principle induce a similar effect within the studied 6 cm from it. However, the effect was seen for all bed forms, also the glass bed, and the first reason hence probably the dominant one. This means that the experiments did not reflect idealized hydraulic conditions, which on the other hand was not the purpose of the experiments. The purpose was to study non-ideal conditions which are not uncommon in the real world. Table 1 summarizes the flow turbulence characteristics measured during each experiment. The flow characteristics could not be measured for the cohesive sediment bed experiments due to the presence of suspended solids in the flow, which made it impossible to solely detect tracer particles.

3.2. Settling and rising velocity of PE particles

The nature of particle motion is determined by the balance between the forces acting upon the particle. In a motionless water column, a

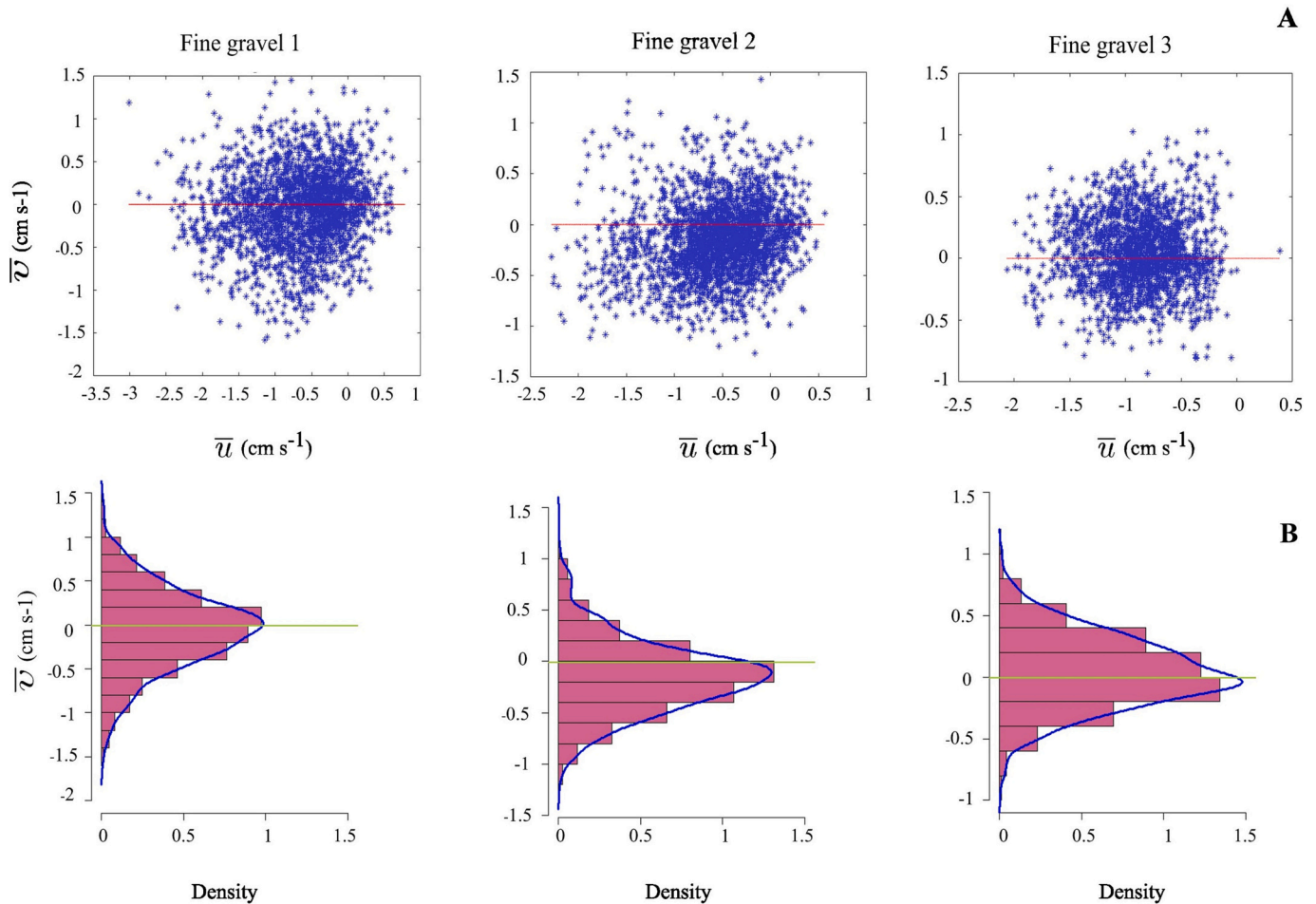


Fig. 2. The mean (tracked average) velocity obtained during 30 s of measurements for PE particles (A). The red line depicts the Stokes rising velocity of a 47 μm PE particle, which was the upper size of the particles tested in this study. I.e., the velocity which would be expected had the flow been completely quiescent. B: Histogram of the mean (tracked average) vertical particle velocity with the estimated density distribution (blue curve). The green line shows the Stokes velocity of a 47 μm PE particle.

freely moving particle's terminal velocity (falling or rising) is defined under the assumption that gravity, buoyancy, and fluid drag are acting on the particle, and these forces are properly in balance. Stokes formulated the first theoretical model relating the terminal velocity of a particle in a liquid to the gravitation and drag forces acting on said particle. Stokes' law provides a convenient measure for calculating particles' settling or rising velocity; however, it applies only to small spherical particles existing in laminar flow, i.e., low Reynolds numbers (Stokes, 1851).

Fig. 2 shows the measured time-averaged velocities of the PE particles for the fine gravel bed at different flow conditions (the full set of experiments is shown in supplementary information, Fig. S2). \bar{v} and \bar{u} denote respectively the average vertical and horizontal velocity of each tracked PE particle (blue stars in Fig. 2A). The measured vertical velocity of particles deviated substantially from the Stokes velocity. The Stokes terminal velocity for the tested MPs (40–47 μm) was between -0.000434 and -0.000599 cm s^{-1} , meaning the particles had positive buoyancy in quiescent water and would have risen towards the water surface at 0.000434 – 0.000599 cm s^{-1} . However, in the experiments the tracked PE particles showed both positive and negative vertical velocity (Figs. 2A, B, and S2.), meaning some particles moved towards the bed and some towards the water surface. Moreover, the numerical particle velocity was magnitudes above what would be expected for quiescent water as predicted by Stokes law.

A dimensionless parameter (Z) was defined as the relative ratio of the effective value \bar{v} (average vertical velocity of all tracked PE particles in an experiment) measured in each flow regime to that expected in quiescent water (Stokes velocity) for 47 μm particles, i.e., the upper size of the particles added to the flow. Thus, values of $Z > 1$ indicate "enhanced" average rising rates (particles moving towards the surface), and $Z < 1$ diminished average rising rates or enhanced downward movement (particles moving towards the bed).

For all bed types and flow intensities, the average particle velocity deviated substantially from the predicted Stokes velocity (Table S1 and Fig. S3). No clear enhancement or diminishment pattern was observed for the different tested conditions. Medium sand 3 (TKE = 0.000625 J/kg) had the highest average enhancement of downward movement ($Z < 1$), namely 255. I.e., the numerical value of the average particle velocity deviated 255 times from the intrinsic Stokes rising velocity. For this test condition, the particle with the most extreme downward movement had a velocity of 1.19 cm s^{-1} , that is, 1987 times higher than expected Stokes velocity and in the opposite direction of it. For the fine gravel bed 2 (TKE = 0.0008 J/kg), particles were on average moving towards the surface 250 times faster than predicted by Stokes law.

This finding implies that even though the average velocity was either upwards or downwards, there was in each cohort of particles always individual velocities in the downwards (or upwards) direction with $Z \gg 1$ or $Z \ll 1$ (Table S1 and Fig. S3). In other words, even in flow regimes where the net transport was upwards, many single particles were conveyed towards the bed. Such phenomenon was also reported by Kukulka et al. (2012) who observed that wind-driven turbulent mixing within the surface boundary layer in the ocean transferred and redistributed buoyant MPs lower in the water column and hence reduced the surface concentration. Rapid conveyance of particles towards the bed (downward movement) and towards the surface (upward movement) was hence driven by flow eddies. Such movement can sweep particles along and give them an increased momentum. When a flow eddy interacts with the bed, the inertia of a particle it carries can cause it to leave the diverted flow eddy and get into physical contact with the bed, where it may become immobilized. On the other hand, such flow eddies might also cause ejection of particles as they get swept off the bed. Whether a particle sticks to the bed would depend on both particle and bed characteristics. In a coarse bed, for example, a particle might get carried into the bed and get immobilized in its pores (Phillips et al., 2019). In a finer bed, the particle might adhere to the bed due to cohesive forces (Arnon et al., 2010).

The effect of different turbulence conditions on the vertical velocity distribution of PE particles is shown in Fig. S4. For each of the three conditions, the variability of particle velocities around the median velocity was quite similar, indicating that the bed type did not significantly affect the pattern of particle movement (Fig. S4). Neither did the bed type affect the median of the movement. There was, however, a clear decrease in the variation of particle velocity with decreasing turbulence. At high turbulence rates, more eddies with higher energy occurred, imposing larger random flow fluctuations. This then resulted in higher extreme values of upward and downward particle velocity.

3.3. Generic prediction of particle transport mode and fate

Turbulent motions in the flow can induce mixing of suspended particles, here MPs, if the turbulence intensity is notably larger than the rising or settling velocity of the particle. Somewhat counterintuitive, this means that particles of a density lower than that of water will not necessarily be found predominantly at the water surface, and particles of a density higher than that of water will not necessarily be found predominantly at the bed. Whether a lighter than water particle will mainly be at the water surface, or a heavier than water particle mainly at the bed, depends on both the properties of the MP and the vertical mixing.

Crucial MP properties cover size, shape, and density, while the properties of the flow include the turbulent shear velocity. The Rouse parameter (P) was used to quantify where in the flow a particle will be most likely to occur. P is a dimensionless parameter used to describe the relative significance of inertial vertical movements of particles due to gravity and buoyancy compared to turbulent-induced particle entrainment (Rouse, 1937). It represents the ratio between the rising/settling ability of a particle versus its vertical motion due to turbulent mixing and integrates the effects of particle size and density with the intensity of a turbulent shear flow (Eq. (3)). The application of the Rouse parameter for buoyant and non-buoyant plastic particles has been confirmed by Cowger et al. (2021) and Born et al. (2023). When the shear velocity is low, the particle distribution in the water column is expected to be mainly governed by the rising or settling ability of the particles, whereas turbulent mixing plays a minor role. When the shear velocity is high, the distribution is expected to be mainly governed by turbulent mixing, i.e., the particles tend to be evenly distributed in the flow irrespective of their size and density.

Cowger et al. (2021) stated that $P < -2.5$ characterizes surface load particles (travelling only at the surface); $-2.5 < P < -0.8$ characterizes rising suspended load particles (partially distributed throughout the water column with higher concentrations at the surface); $0.8 > P > -0.8$ characterizes wash load particles (equally distributed throughout the water column); $2.5 > P > 0.8$ characterizes settling suspended load particles (partially distributed throughout the water column with higher concentrations at the bed); $7.5 > P > 2.5$ characterizes bed load particles (moving primarily along the bed by rolling, skipping, and saltating along the bottom-most portion of the flow field); and $P > 7.5$ characterizes immobile particles (in contact with the bed and not moving). In the present work, three flow conditions were assessed experimentally for spherical PE particles of 40–47 μm . Applying the Rouse parameter, these results were extrapolated to cover particles of 10–1000 μm and densities of 880–1550 kg m^{-3} at the highest and lowest shear velocity measured.

The effect of increasing turbulence intensity on the particle's transport is shown in Fig. 3. For illustration purposes, the upper size range of the PE particles of the current study (47 μm) is indicated by a star. With increasing turbulence intensity, a wider range of particles can be transported as wash load. This means that larger particles with higher densities can be kept in suspension due to the mixing caused by eddies, and hereby overcome the gravitational force acting on them. Particles with a density close to that of water would occur as wash load in a wider size range, regardless of turbulence intensity. For example, a 250 μm PE particle (995 kg m^{-3}) and 250 μm PS particle 1040 kg m^{-3} would behave quite similarly at all tested turbulence levels. Regardless of their

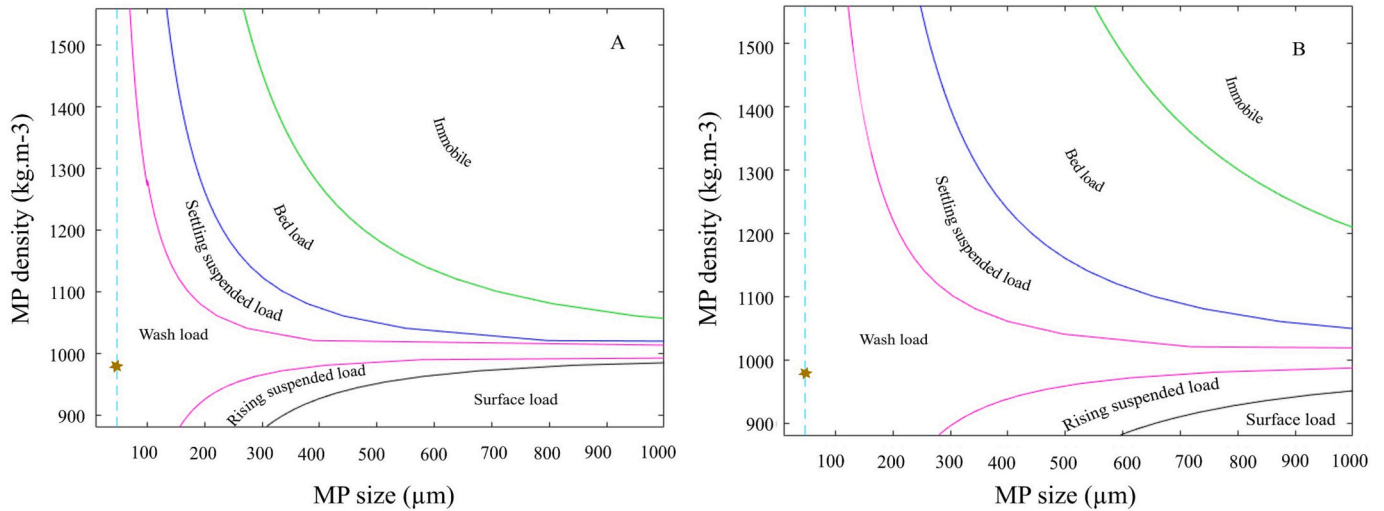


Fig. 3. Rouse domains for lowest (A) and highest measured shear velocity (B). The star shows the location of a 47 µm PE particle in the Rouse domain (the upper size of PE particles used). The vertical turquoise line shows particles with different densities and 47 µm diameter.

densities, these would all occur as wash load for the tested shear velocities, meaning that all such particles would be distributed over the full water depth. Non-spherical particles would be even less affected by their density as the settling velocity of a non-spherical particle is lower than that of a spherical particle of the same mass (Wang et al., 2021).

While the impact of density on the motion of small particles is not significant, it does become significant for larger particles. Considering for example PVC particles of 1150 kg m⁻³ and 500 µm size under the highest turbulence intensity condition (Fig. 3B): While a portion of these particles would stay in the water column due to turbulent mixing, a larger fraction would be close to the bed and moving as settling suspended load. At the lowest turbulence intensity, these particles would be at the bed and transported as bed load (Fig. 3A). For similar reasons, for example 500 µm PE particles (940 kg m⁻³) would at the highest turbulence intensity move as rising suspended load while they would float at the water surface (surface load) at the lowest turbulence intensity. Turbulence would, in other words, be insufficient to pull them down (Fig. 3).

This is in accordance with the findings of DiBenedetto et al. (2023) who investigated MP segregation by rising of buoyant MPs under strong winds (wind-driven turbulence) in the ocean surface mixed layer. The authors stated that physical characteristics of the MPs will also control

their vertical distribution. DiBenedetto et al. (2023) showed that MPs with high rising velocity were more abundant at the ocean surface, and turbulent mixing was unable to entrain them far below the surface. MPs with lower rising velocity were, on the other hand, well mixed in the free surface boundary layer at the same turbulence condition. Similarly, the findings of Kooi et al. (2016) showed that not all types of MP behaved the same while in the ocean. Less buoyant MPs tended for example to be mixed deeper than more buoyant ones. They also suggested that vertical distribution of buoyant MPs not only depends on environmental conditions, but also on their size and shape.

3.4. PE particles trajectories

The spatial movement of the PE particles were tracked to gain insights into particle movement patterns and entrainment behavior (fluid-particle interactions) in response to factors such as changes in fluid velocity and turbulence. Fig. 4 shows the trajectories which reached the lowest ~6 cm of the flume for the gravel bed at different flow conditions. The particle trajectory patterns were similar for repetitions of the experiment under identical flow and bed type conditions. For reasons of clarity, only 1 repetition (30 s of measurement) is hence shown (further instances of repetitions and other bed types are shown in Fig. S5).

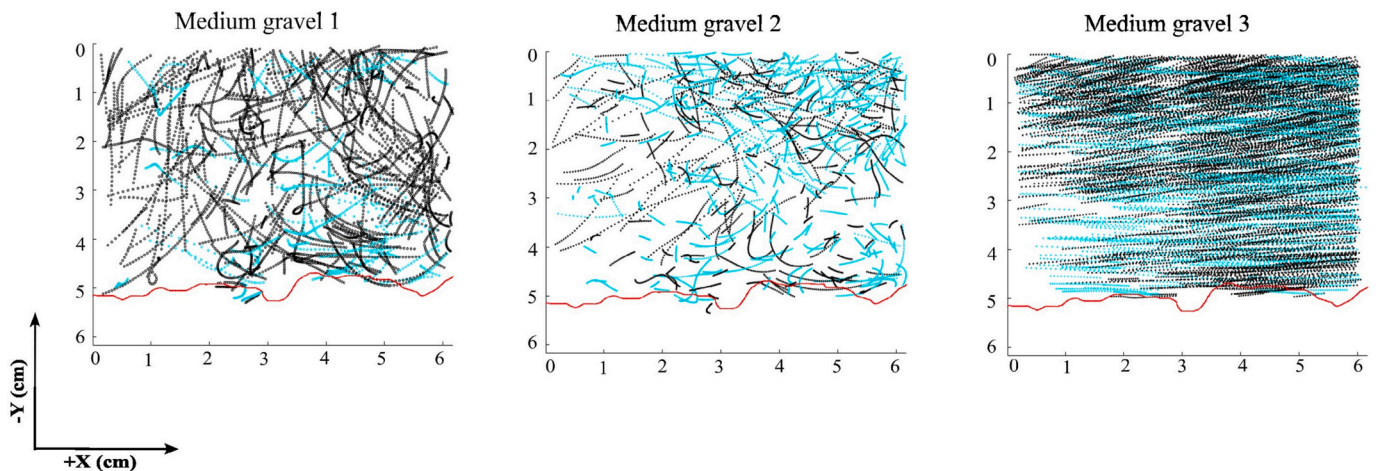


Fig. 4. Selected particle trajectories from one of the six repetitions (30 s) for the medium gravel bed. The first, second, and third illustration show trajectories for flow conditions 1, 2, and 3, respectively. Particle trajectories in black move towards the bed and trajectories in turquoise move towards the surface. The flow direction is from right to left. The red lines show the bed topographies.

For each flow condition, the pattern of particle trajectories was similar regardless of the bed type. At flow condition 1, i.e., where the pump was at its highest flow rate, particle motion was quite chaotic, and particles followed seemingly random trajectories. Most particles could not be followed all the 6 cm which the laser sheet covered in the y-x directions, as they moved out of the plane (i.e., in the z-direction). At flow condition 2, the particle trajectories were still erratic. At flow condition 3, particles followed smooth semi-parallel trajectories. Moreover, particles could be tracked over longer distance before disappearing and their trajectories ended, indicating that particles were moving longer in the x-y plane (laser sheet) in the observation period.

3.5. Interaction between particles and bed

While the turbulence caused particles to move vertically at velocities higher than their intrinsic settling/rising velocity, this did not tell whether they physically touched the bed and hence experienced a finite probability of becoming immobilized at the bed. The rate at which the particles arrived at the beds hence remained unknown. To assess this, and since the first prerequisite for a particle to encounter the bed is that it must move towards it, the abundance of tracked particles moving towards the bed in the 3 min of measurement time was calculated.

The highest and lowest number of particles moving downward were seen for medium sand 3 and fine gravel 2 with 66 % and 30 %, respectively. The abundance of sinking and rising PE particles at different test beds and flow conditions is displayed in Fig. S6 of the supplementary information. For all flow conditions and bed types, there hence was a significant number of particles moving towards the bed within the field of view, albeit no clear trend could be found with the shear velocity (u^*) and the bed type. To get closer to assessing the rate of particle/bed encounters, a near-bed zone was defined as a region 2 mm from the bed (bed zone). The median percentage of particles in the field of view reaching the bed zone within the 3 min was 4.2 %, with highest and lowest values of 0.8 % and 8.8 % for the glass bed 3 and medium

gravel 2, respectively. I.e., even though the Rouse parameter indicated that the MPs were conveyed as wash-load, they still had a quite significant probability of getting into contact with the bed. Trajectories of particles coming in close contact with the bed are exemplified in Fig. 5. The full set is shown in Supplementary Information Fig. S7.

Assuming an infinitely long flume, and that particles are not resupplied, this would lead to around 99 % of all beads in the flow getting into close contact with the bed within a day. Although the particles tracked in the bed zone had the highest probability of hitting the bed and thus potentially getting trapped by the bed, the experiments were not designed to quantify how many of the close encounters resulted in physical contact with the bed. Nevertheless, the experiments illustrate how turbulent particle movement can lead to entrapment of microplastics within a rather short time span.

While the experiments were done in the waters of a slow flowing flume, the general conclusion on turbulence-driven MP transport holds true for any water body which exhibits a similar turbulence regime (McWilliams and Sullivan, 2000). Whether the turbulence is induced by the flow of water in a channel or waves of an open water body (Chor et al., 2018), the conclusions of eddies driving the transport of MPs holds true. In a shallow lake, for example, where wind and waves cause turbulence all the way to the lakebed (Reardon et al., 2014), the eddies may transport lighter-than-water MPs to the bed where they may become immobilized. In the open ocean where the upper water layer is completely mixed, turbulent eddies may transport such particles towards the deeper quiescent water layers where flow is laminar (Brunner et al., 2015). Once there, the lighter-than-water MPs would have to shift to a different transport mode to reach the bottom, for example ballasted settling due to biofilm growth and/or particle coagulation (Galgani et al., 2022). While turbulence alone hence cannot explain why MPs reach the deep ocean floor, it is crucial in understanding the processes in the upper water layers. Without this understanding and including it in MP transport models, these would struggle to predict MP transport accurately (Onink et al., 2022). This would lead to poorer predictions of MP pathways and their final destination, which then would lead to poorer assessment of the impacts these MPs can have on the environment.

4. Conclusion

The vertical transport velocities of 40–47 μm PE particles ($\rho = 995 \text{ kg m}^{-3}$) in a flume ($1.85\text{--}4.17 \text{ cm s}^{-1}$) were orders of magnitude above the rising velocity as calculated by Stokes law ($0.43\text{--}0.6 \mu\text{m s}^{-1}$). Within the investigated 6 cm of the bed, both the upwards and downwards velocity of individual MPs reached as much as 2.4 cm s^{-1} . There was no clear preference for these lighter-than-water particles to either rise or sink. Zooming in on the 2 mm closest to the bed showed that some particles came into close encounters with, or even hit, the bed. Together this illustrated that the eddies generated in the flume overcame the rising tendency of the MPs and brought them to the bottom part of the flume where they could be captured by the bed.

Applying the results to well-established particle transport theory presented an approach to predict MP distribution in a turbulent water body. The results however also showed that these yield average distributions only. Even though a MP on average is predicted to stay suspended in the water, turbulence causes eddies, which sometimes can convey such an MP close to the bed where it might become immobilized. The study clearly showed that the fate of MPs in turbulent waters is linked to turbulent transport, which hence must be considered when predicting the transport and fate of MPs in aquatic environments and for developing strategies to mitigate their impact on the ecosystem. To predict the pathways of MPs in aquatic environments and their final destinations, it is essential to comprehend the influence of turbulence. This understanding will in turn lead to improved predictions of local concentrations and, consequently, provide a better understanding of their environmental impacts.

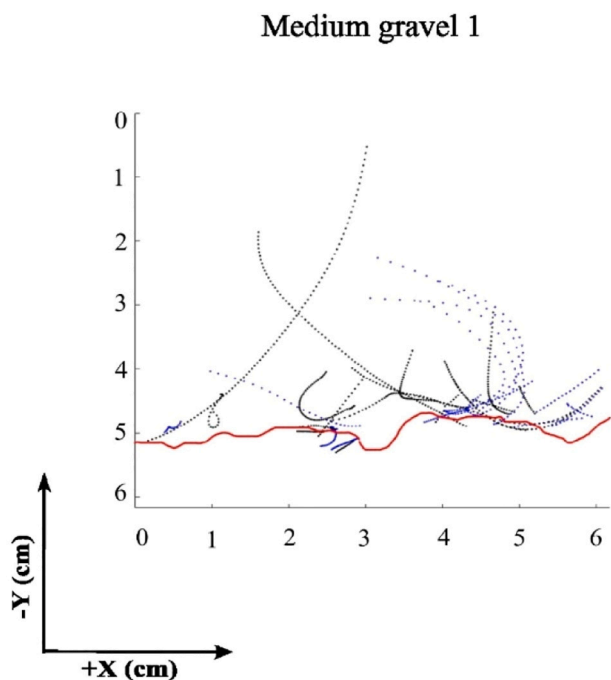


Fig. 5. Examples of PE particles which within a 30 s measuring window had been within 2 mm of the bed. Particles with trajectories shown in black moved towards the bed and those in blue moved away from it (some of these particles might have hit the bed and bounced off it). The red line shows the bed topography.

CRediT authorship contribution statement

Marziye (Shabnam) Molazadeh carried out the experiments, interpreted the results, and wrote the original draft. Guilherme Calabro helped with carrying out the experiments. Fan Liu, Rachid Dris and Bruno Tassin co-supervised the project. Andreas Lorke and Lorenzo Rovelli providing resources. Jes Vollertsen supervised the project. All authors contributed to the final manuscript.

Declaration of competing interest

The authors declare no competing interests.

Data availability

Data will be made available on request.

Acknowledgements

This work was carried out within the Limnoplant project. This project has received funding from the European Union's Horizon 2020 research and innovation programme under grant agreement No 860720. The authors wish to thank Bruno J. Lemaire and Cedric Chaumont from INRAE to provide the hydraulic lab.

Appendix A. Supplementary data

Supplementary data to this article can be found online at <https://doi.org/10.1016/j.scitotenv.2023.168540>.

References

- Andrady, A.L., 2011. Microplastics in the marine environment. *Mar. Pollut. Bull.* 62, 1596–1605. <https://doi.org/10.1016/j.marpolbul.2011.05.030>.
- Arnon, S., Marx, L.P., Searcy, K.E., Packman, A.I., 2010. Effects of overlying velocity, particle size, and biofilm growth on stream-subsurface exchange of particles. *Hydrol. Process.* 24 (1), 108–114. <https://doi.org/10.1002/hyp.7490>.
- Ballent, A., Pando, S., Purser, A., Juliano, M.F., Thomsen, L., 2013. Modelled transport of benthic marine microplastic pollution in the Nazaré Canyon. *Biogeosciences* 10 (12), 7957. <https://doi.org/10.5194/bg-10-7957-2013>.
- Besseling, E., Quik, J.T.K., Sun, M., Koelmans, A.A., 2017. Fate of nano- and microplastic in freshwater systems: a modeling study. *Environ. Pollut.* 540–548, 220. <https://doi.org/10.1016/j.envpol.2016.10.001>.
- Born, M.P., Brulle, C., Schaefer, D., Hillebrand, G., Schuttrumpf, H., 2023. Determination of microplastics' vertical concentration transport (rouse) profiles in flumes. *Environ. Sci. Technol.* 57, 5569–5579. <https://doi.org/10.1021/acs.est.2c06885>.
- Brunner, K., Kukulka, T., Proskurowski, G., Law, K.L., 2015. Passive buoyant tracers in the ocean surface boundary layer: 2. Observations and simulations of microplastic marine debris. *J. Geophys. Res. Oceans* 120 (11), 7559–7573. <https://doi.org/10.1002/2015JC010840>.
- Chamecki, M., Chor, T., Yang, D., Meneveau, C., 2019. Material transport in the ocean mixed layer: recent developments enabled by large eddy simulations. *Rev. Geophys.* 57, 1338–1371.
- Chor, T., Yang, D., Meneveau, C., Chamecki, M., 2018. A turbulence velocity scale for predicting the fate of buoyant materials in the oceanic mixed layer. *Geophys. Res. Lett.* 45 (21), 11817–11826. <https://doi.org/10.1029/2018GL080296>.
- Cole, M., Lindeque, P., Halsband, C., Galloway, T.S., 2011. Microplastics as contaminants in the marine environment: a review. *Mar. Pollut. Bull.* 62, 2588–2597. <https://doi.org/10.1016/j.marpolbul.2011.09.025>.
- Cowger, W., Gray, A.B., Güllinger, J.J., Fong, B., Waldschlager, K., 2021. Concentration depth profiles of microplastic particles in river flow and implications for surface sampling. *Environ. Sci. Technol.* 55, 6032–6041. <https://doi.org/10.1021/acs.est.1c01768>.
- Daily, J., Hoffman, M.J., 2020. Modelling the three-dimensional transport and distribution of multiple microplastic polymer types in Lake Erie. *Mar. Pollut. Bull.* 154 (111024), 0025–326X. <https://doi.org/10.1016/j.marpolbul.2020.111024>.
- De Leeuw, J., Lamb, M.P., Parker, G., Moodie, A.J., Hought, D., Venditti, J.G., Nittrouer, J.A., 2020. Entrainment and suspension of sand and gravel. *Earth Surf. Process. Landf.* 8, 485–504. <https://doi.org/10.5194/esurf-8-485-2020>.
- DiBenedetto, M.H., Donohue, J., Tremblay, K., Edson, E., Law, K.L., 2023. Microplastic segregation by rise velocity at the ocean surface. *Environ. Res. Lett.* 18, 024036. <https://doi.org/10.1088/1748-9326/acb505>.
- Dietrich, W.E., 1982. Settling velocity of natural particles. *Water Resour. Res.* 18 (6), 1615–1626. <https://doi.org/10.1029/WR018i06op01615>.
- Galgani, L., Gossmann, I., Scholz-Boettcher, B., Jiang, X.T., Liu, Z.F., Scheidemann, L., Schlundt, C., Engel, A., 2022. Hitchhiking into the deep: how microplastic particles are exported through the biological carbon pump in the North Atlantic Ocean. *Environ. Sci. Technol.* 56 (22), 15638–15649. <https://doi.org/10.1021/acs.est.2c04712>.
- Isachenko, I., 2020. Catching the variety: Obtaining the distribution of terminal velocities of microplastics particles in a stagnant fluid by a stochastic simulation. *Mar. Pollut. Bull.* 159, 111464. <https://doi.org/10.1016/j.marpolbul.2020.111464>.
- Isobe, A., Iwasaki, S., 2022. The fate of missing ocean plastics: are they just a marine environmental problem? *Sci. Total Environ.* 825, 153935. <https://doi.org/10.1016/j.scitotenv.2022.153935>.
- Jalón-Rojas, I., Romero-Ramirez, A., Fauquemberge, K., Rossignol, L., Cachot, J., Sous, D., Morin, B., 2022. Effects of biofilms and particle physical properties on the rising and settling velocities of microplastic fibers and sheets. *Environ. Sci. Technol.* 56, 8114–8123. <https://doi.org/10.1021/acs.est.2c01302>.
- Kaiser, D., Estelmann, A., Kowalski, N., Glockzin, M., Waniek, J.J., 2019. Sinking velocity of sub-millimeter microplastic. *Mar. Pollut. Bull.* 139, 214–220. <https://doi.org/10.1016/j.marpolbul.2018.12.035>.
- Khatmullina, L., Chubarenko, I., 2019. Transport of marine microplastic particles: why is it so difficult to predict? *Anthropocene Coasts* 2 (1), 293–305. <https://doi.org/10.1139/anc-2018-0024>.
- Khatmullina, L., Isachenko, I., 2017. Settling velocity of microplastic particles of regular shapes. *Mar. Pollut. Bull.* 114 (2), 871–880. <https://doi.org/10.1016/j.marpolbul.2016.11.024>.
- Koelmans, A.A., Redondo-Hasselerharm, P.E., Nor, N.H.M., et al., 2022. Risk assessment of microplastic particles. *Nat. Rev. Mater.* 7, 138–152. <https://doi.org/10.1038/s41578-021-00411-y>.
- Kooi, M., Reisser, J., Slat, B., Ferrari, F.F., Schmid, M.S., Cunsolo, S., Brambini, R., Nobel, K., Sirks, L.A., Linders, T.E.W., Schoeneich-Argent, R.I., Koelmans, A.A., 2016. The effect of particle properties on the depth profile of buoyant plastics in the ocean. *Sci. Report.* 33882. <https://doi.org/10.1038/srep33882>.
- Kowalski, N., Reichardt, A.M., Waniek, J.J., 2016. Sinking rates of microplastics and potential implications of their alteration by physical, biological, and chemical factors. *Mar. Pollut. Bull.* 109 (1), 310–319. <https://doi.org/10.1016/j.marpolbul.2016.05.064>.
- Kukulka, T., Proskurowski, G., Moret-Ferguson, S., Meyer, D.W., Law, K.L., 2012. The effect of wind mixing on the vertical distribution of buoyant plastic debris. *Geophys. Res. Lett.* 39, L07601. <https://doi.org/10.1029/2012GL051116>.
- Li, Y., Wang, X., Fu, W., Xia, X., Liu, C., Min, J., Zhang, W., Crittenden, J.C., 2019. Interactions between nano/micro plastics and suspended sediment in water: implications on aggregation and settling. *Water Res.* 161, 486–495. <https://doi.org/10.1016/j.watres.2019.06.018>.
- Liu, F., Vianello, A., Vollertsen, J., 2019. Retention of microplastics in sediments of urban and highway stormwater retention ponds. *Environ. Pollut.* 255, 113335. <https://doi.org/10.1016/j.envpol.2019.113335>.
- Liang, J.-H., McWilliams, J.C., Sullivan, P.P., Baschek, B., 2012. Large eddy simulation of the bubbly ocean: new insights on subsurface bubble distribution and bubble-mediated gas transfer. *J. Geophys. Res.-Oceans* 117, C04002. <https://doi.org/10.1029/2011JC007766>.
- Liu, Y., Lorenz, C., Vianello, A., Syberg, K., Nielsen, A.H., Nielsen, T.G., Vollertsen, J., 2023. Exploration of occurrence and sources of microplastics (>10 µm) in Danish marine waters. *Sci. Total Environ.* 865, 0048–9697. <https://doi.org/10.1016/j.scitotenv.2022.161255>.
- Long, M., Moriceau, B., Gallinari, M., Lambert, C., Huvet, A., Raffray, J., Soudant, P., 2015. Interactions between microplastics and phytoplankton aggregates: impact on their respective fates. *Mar. Chem.* 175, 39–46. <https://doi.org/10.1016/j.marchem.2015.04.003>.
- Lu, X., Wang, X., Liu, X., Singh, V.P., 2023. Dispersal and transport of microplastic particles under different flow conditions in riverine ecosystem. *J. Hazard. Mater.* 442, 0304–3894. <https://doi.org/10.1016/j.jhazmat.2022.130033>.
- MathWorks. https://www.mathworks.com/products/new_products/release2020a.html.
- McWilliams, J.C., Sullivan, P.P., 2000. Vertical mixing by Langmuir circulations. *Spill Sci. Technol. Bull.* 6 (3–4), 225–237. [https://doi.org/10.1016/S1353-2561\(01\)00041-X](https://doi.org/10.1016/S1353-2561(01)00041-X).
- Molazadeh, M., Liu, F., Simon-Sánchez, L., Vollersten, J., 2023. Buoyant microplastics in freshwater sediments – how do they get there? *Sci. Total Environ.* 860 (160489), 0048–9697. <https://doi.org/10.1016/j.scitotenv.2022.160489>.
- Moore, C.J., 2008. Synthetic polymers in the marine environment: a rapidly increasing, long-term threat. *Environ. Res.* 108 (2), 131–139. <https://doi.org/10.1016/j.envres.2008.07.025>.
- Olesen, K.B., Stephansen, D.A., van Alst, N., Vollertsen, J., 2019. Microplastics in a stormwater pond. *Water (Switzerland)* 11 (7), 1466. <https://doi.org/10.3390/w11071466>.
- Onink, V., van Sebille, E., Laufkotter, C., 2022. Empirical Lagrangian parametrization for wind-driven mixing of buoyant particles at the ocean surface. *Geosci. Model Dev.* 15 (5), 1995–2012. <https://doi.org/10.5194/gmd-15-1995-2022>.
- Phillips, C.B., Dallmann, J.D., Jerolmack, D.J., Packman, A.I., 2019. Fine-particle deposition, retention, and resuspension within a sand-bedded stream are determined by streambed morphodynamics. *Water Resour. Res.* 55 (12), 10303–10318. <https://doi.org/10.1029/2019WR025272>.
- Reardon, K.E., Bombardelli, F.A., Moreno-Casas, P.A., Rueda, F.J., Schladow, S.G., 2014. Wind-driven nearshore sediment resuspension in a deep lake during winter. *Water Resour. Res.* 50 (11), 8826–8844. <https://doi.org/10.1002/2014WR015396>.
- Reisser, J.W., Slat, B., Noble, K.D., Plessis, K.D., Epp, M., Proietti, M.C., de Sonnevill, J., Becker, T., Pattiaratchi, C., 2015. The vertical distribution of buoyant plastics at sea: an observational study in the North Atlantic Gyre. *Biogeosciences* 12, 1249–1256. <https://doi.org/10.5194/bg-12-1249-2015>.

- Reynolds, O., 1895. On the dynamical theory of incompressible viscous fluids and the determination of the criterion. *Philos. Trans. R. Soc. Lond.* 186, 123–164. <https://doi.org/10.1098/rsta.1895.0004>.
- Rouse, H., 1937. Modern conceptions of the mechanics of fluid turbulence. *Trans. Am. Soc. Civ. Eng.* 102, 463–505. <https://doi.org/10.1061/TACEAT.0004872>.
- Semcesen, O.P., Wells, G.M., 2021. Biofilm growth on buoyant microplastics leads to changes in settling rates: implications for microplastic retention in the Great Lakes. *Mar. Pollut. Bull.* 170, 112573 <https://doi.org/10.1016/j.marpolbul.2021.112573>.
- Shamskhany, A., Karimpour, S., 2022. Entrainment and vertical mixing of aquatic microplastics in turbulent flow: the coupled role of particle size and density. *Mar. Pollut. Bull.* 184 (114160), 0025–326X. <https://doi.org/10.1016/j.marpolbul.2022.114160>.
- Simon-Sanchez, L., Grelaud, M., Franci, M., Ziveri, P., 2022. Are research methods shaping our understanding of microplastic pollution? A literature review on the seawater and sediment bodies of the Mediterranean Sea. *Environ. Pollut.* 292, 118275 <https://doi.org/10.1016/j.envpol.2021.118275>.
- Stokes, G.G., 1851. On the effect of the internal friction of fluids on the motion of pendulum. *Pitt. Press* 9, 1. <https://doi.org/10.1017/CBO9780511702266.002>.
- Taylor, J.R., 2018. Accumulation and subduction of buoyant material at submesoscale fronts. *J. Phys. Oceanogr.* 48, 1233–1241.
- Thielicke, W., Stamhuis, E., 2014. PIVlab—towards user-friendly, affordable, and accurate digital particle image velocimetry in MATLAB. *J. Open Res. Softw.* 2, 1. <https://doi.org/10.5334/jors.bl>. https://web.stanford.edu/~nto/software_tracking.shtml/ (accessed 25 July 2023).
- Waldschläger, K., Schüttrumpf, H., 2019. Effects of Particle Properties on the Settling and Rise Velocities of Microplastics in Freshwater under Laboratory Conditions. *Environ. Sci. Technol.* 53 (4), 1958–1966.
- Wang, Z., Dou, M., Ren, P.J., Sun, B., Jia, R.P., Zhou, Y.Z., 2021. Settling velocity of irregularly shaped microplastics under steady and dynamic flow conditions. *Environ. Sci. Pollut. Res.* 28 (44), 62116–62132. <https://doi.org/10.1007/s11356-021-14654-3>.
- Yan, M., Yang, J., Sun, H., Liu, C., Wang, L., 2022. Occurrence and distribution of microplastics in sediments of a man-made lake receiving reclaimed water. *Sci. Total Environ.* 83, 0048–9697. <https://doi.org/10.1016/j.scitotenv.2021.152430>.
- Yang, D., Chamecki, M., Meneveau, C., 2014. Inhibition of oil plume dilution in Langmuir ocean circulation. *Geophys. Res. Lett.* 41, 1632–1638.